The Astrophysical Journal Letters, 708:L47–L51, 2010 January 1 doi:10.1088/2041-8205/708/1/L47

QUASI-PERIODIC PULSATIONS IN THE GAMMA-RAY EMISSION OF A SOLAR FLARE

V. M. Nakariakov[1], C. Foullon[1], I. N. Myagkova[2], and A. R. Inglis[1]
[1] Physics Department, University of Warwick, Coventry, CV4 7AL, UK; V.Nakariakov@warwick.ac.uk
[2] Skobeltsyn Institute of Nuclear Physics, Lomonosov Moscow State University, Moscow 119992, Russia
Received 2009 September 17; accepted 2009 December 1; published 2009 December 16

ABSTRACT

Quasi-periodic pulsations (QPPs) of gamma-ray emission with a period of about 40 s are found in a single loop X-class solar flare on 2005 January 1 at photon energies up to 2–6 MeV with the SOlar Neutrons and Gamma-rays (SONG) experiment aboard the CORONAS-F mission. The oscillations are also found to be present in the microwave emission detected with the Nobeyama Radioheliograph, and in the hard X-ray and low energy gamma-ray channels of RHESSI. Periodogram and correlation analysis shows that the 40 s QPPs of microwave, hard X-ray, and gamma-ray emission are almost synchronous in all observation bands. Analysis of the spatial structure of hard X-ray and low energy (80–225 keV) gamma-ray QPP with RHESSI reveals synchronous while asymmetric QPP at both footpoints of the flaring loop. The difference between the averaged hard X-ray fluxes coming from the two footpoint sources is found to oscillate with a period of about 13 s for five cycles in the highest emission stage of the flare. The proposed mechanism generating the 40 s QPP is a triggering of magnetic reconnection by a kink oscillation in a nearby loop. The 13 s periodicity could be produced by the second harmonics of the sausage mode of the flaring loop.

Key words: Sun: flares – Sun: oscillations – Sun: X-rays, gamma rays

Online-only material: color figures

1. INTRODUCTION

Quasi-periodic pulsations (QPPs) are a frequently observed feature of solar and stellar flaring emission. The typical periods range from sub-second scales to several minutes (see Nakariakov 2007; Nakariakov & Melnikov 2009). QPPs are often observed in non-thermal emission associated with accelerated electrons, e.g., via gyrosynchrotron in microwave and bremsstrahlung in hard X-ray. Microwave and hard X-ray QPPs are usually observed to be in phase (e.g., Asai et al. 2001; Grechnev et al. 2003; Dauphin et al. 2005; Inglis & Nakariakov 2009). The physical mechanism responsible for the generation of QPPs remains unknown. The possible non-exclusive options include the modulation of electron dynamics by magnetohydrodynamic (MHD) oscillations (e.g., Zaitsev & Stepanov 1982), periodic triggering of energy releases by MHD waves (Foullon et al. 2005; Nakariakov et al. 2006), MHD flow overstability (Ofman & Sui 2006), and oscillatory regimes of magnetic reconnection (Kliem et al. 2000; Murray et al. 2009); shorter period QPPs in the radio band can be associated with wave–particle interactions (Aschwanden 1987). Important information can be gained by comparing light curves or images in different emission bands, which relate to different emission mechanisms. Our understanding of those physical mechanisms, e.g., magnetic reconnection and particle acceleration, is incomplete without revealing mechanisms for QPP generation. Moreover, understanding QPP can shed light on the basic physics of solar and stellar flares, by imposing additional constraints on theoretical models.

The manifestation of QPP varies in the spectrum of the electromagnetic emission generated by flares. The flaring hard X-ray emission during individual peaks is found to display a soft-hard-soft spectral evolution (e.g., Grigis and Benz 2004), while in microwaves the soft-hard-harder or even hard-soft-hard evolution can occur (Melnikov & Magun 1998). Furthermore, it is interesting to know how flaring emission in the high energy part of the spectrum, gamma-rays, in particular, manifest QPP. Early observations of solar flare gamma-ray emission showed the presence of QPPs in light curves (e.g., Chupp 1983), however, to the best of our knowledge there has not been any dedicated study of gamma-ray QPPs. Emission in the gamma-ray band, from 0.5 MeV to 10 MeV, is believed to be associated with nuclear processes, e.g., de-excitation, neutron capture, and positron annihilation, caused by flare accelerated ions. Hence QPP in this band would provide flare models with additional challenges (e.g., Aschwanden 2002) and can contribute to our understanding of particle acceleration and dynamics processes in flares.

Lastly, solar flares are known to induce a geomagnetic field response, e.g., in the form of irregular pulsations P1-3sfe with periods of fractions of seconds to several minutes. Hardening of flare radiation is known to affect the geomagnetic response (e.g., Parkhomov et al. 2006). In particular, the effect of solar gamma-ray bursts differs from the effect of X-ray bursts in the time evolution, extension of frequency spectrum, and increase in geomagnetic pulsation activity. The underlying physical mechanisms are not entirely understood. As the typical parameters of QPP in flares coincide with the periods of flare-induced geomagnetic pulsations, the study of QPPs in gamma-ray flares may provide us with the grounds for testing the existence of resonant effects.

The aim of this Letter is to establish relations between QPPs in microwave, hard X-ray, and gamma-ray emission generated in a solar flare by studying multi-instrument observations and by investigating the available spatial information.

2. DATA

We analyze the flare on 2005 January 1, which peaked at about 00:31 UT at *GOES* level X1.7, from the NOAA active region 10715 located on disk at N03E47. The microwave, hard X-ray, and gamma-ray data were obtained with the Nobeyama Radioheliograph (NoRH; Nakajima et al. 1994) using its 17 GHz and 34 GHz intensity correlation plots, RHESSI (Lin et al. 2002) and the SOlar Neutrons and Gamma-rays experiment (SONG)

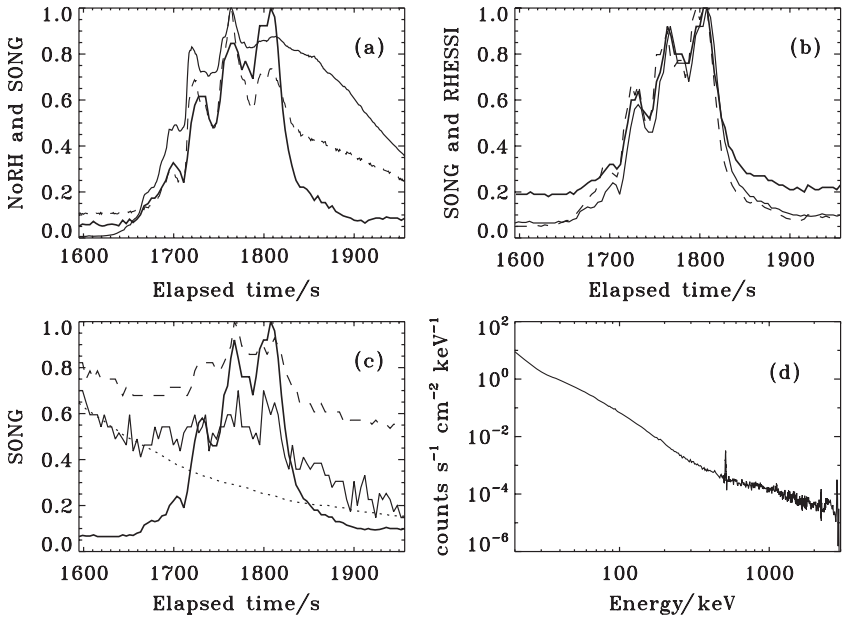

Figure 1. Light curves (correlation plots) normalized to their maximum values for (a) NoRH 17 GHz (solid) and 34 GHz (dashed), and SONG 42–80 keV (thick); (b) SONG 80–225 keV (thin), and RHESSI 50–100 keV (dashed), and 100–300 keV (thick); (c) SONG 80–225 keV (thick), 225–750 keV (dashed), and 2–6 MeV (thin solid); the dashed curve shows the averaged 2–6 MeV light curve from previous orbits. The elapsed time is measured from 00:00 UT on 2005 January 1. (d) Photon energy spectrum integrated between 00:28 UT and 00:32 UT obtained with RHESSI.

on board CORONAS-F (e.g., Myagkova et al. 2007a). The SONG instrument is based on a large CsI(Tl) crystal. Neutrons, hard X-rays, and gamma-rays are recorded by the secondary charged particles. With SONG, the X-ray and gamma-ray emission is measured in 11 channels over the energy range 0.05–200 MeV with the effective area of about 260–280 cm^2. The time cadence of the NoRH data was 1 s and of the SONG data was 3.96 s. Time binning of RHESSI imaging data was 4 s.

Hard X-ray, microwave, and gamma-ray light curves are shown in Figures 1(a)–(c), covering the time interval 00:26:40–00:32:30 UT (1600 to 1950 s from 00:00 UT). Overall, the hard X-ray and microwave light curves are asymmetric, between the gradual growing phase and the following decay phase, which is more abrupt in hard X-rays and more steady in microwaves. In gamma-ray channels of SONG, the flare emission occurs over a gradually decreasing background, connected with the Earth's radiation belts. For the present flare this trend was established from light curves obtained during previous CORONAS-F orbits at the same geographic position (Myagkova et al. 2007b). In both hard X-ray and microwave channels there is clear evidence of QPP with a period of about 40 s and a large modulation depth. Also, the QPP are well seen in the 225–750 keV and 2–6 MeV gamma-ray channels of SONG. The modulation depth of the QPP, calculated as a half of the ratio of the oscillation amplitude to the average low-varying trend, is about 20%–25%. The QPPs are present from the start of the rise phase, at approximately 00:27:30 UT time (1650 s), and last for at least five cycles.

The photon energy spectrum of the flare, obtained with RHESSI by integration over the time interval from 0:28 UT to 0:32 UT, is shown in Figure 1(d). There is clear evidence of the cluster of nuclear lines in the gamma-ray band, e.g., the prominent lines at 511 keV (electron–positron annihilation line) and 2.2 MeV (neutron capture line). Thus, there should be a sufficient amount of accelerated non-thermal ions in the flare, causing the gamma-ray emission.

The spatial structure of X-ray and gamma-ray emission is obtained with RHESSI synthesized images. Contours are overlaid in Figure 2 on a pre-flare EUV coronal image obtained with the Extreme-ultraviolet Imaging Telescope (EIT; e.g., Delaboudinière et al. 1995) at 195 Å and a Michelson Doppler Imager (MDI; e.g., Scherrer et al. 1995) magnetogram. The hard X-ray and gamma-ray emissions have two asymmetric sources situated in regions of opposite magnetic polarity. We shall refer to these sources as upper and lower sources, with positive and negative polarities, respectively. The gamma-ray sources are approximately co-incident with hard X-ray sources. The maximum of the thermal (soft X-ray) emission is situated between the footpoint hard-energy sources. Most likely, those sources are associated with the opposite footpoints of a flaring loop. Thus, the flare can be considered as a standard single loop flare, although the pre-flare EUV image of this active region shows a rather complex loop system. The spatial separation of the sources and hence the flaring loop footpoints, is about 30 arcsec (about 21 Mm). Temporal evolution of the hard X-ray and gamma-ray source asymmetry is discussed in Section 3.3. Note that this event has been included in the statistical study of correlation and asymmetry between solar flare hard X-ray footpoints, based upon the RHESSI data (Jin & Ding 2007, mind, however, the misprint in the event date). In that work, the hard X-ray fluxes at both footpoints were found to be highly correlated. Microwave imaging information is not available because of the low height of the Sun over the horizon.

3. COMPARATIVE ANALYSIS OF MICROWAVE, HARD X-RAY, AND GAMMA-RAY LIGHT CURVES

3.1. Periodogram Analysis

The presence of QPP at all energy levels (17 GHz and 34 GHz of NoRH; 42–80 keV, 80–225 keV, 225–750 keV and 2–6 MeV channels of SONG; and 50–100 keV and 100–300 keV of RHESSI) is confirmed by a periodogram analysis. The slow-varying trend was removed from the light curves in three different fashions: (1) subtracting from the light curve the running average smoothed by 10 points (SONG and RHESSI)

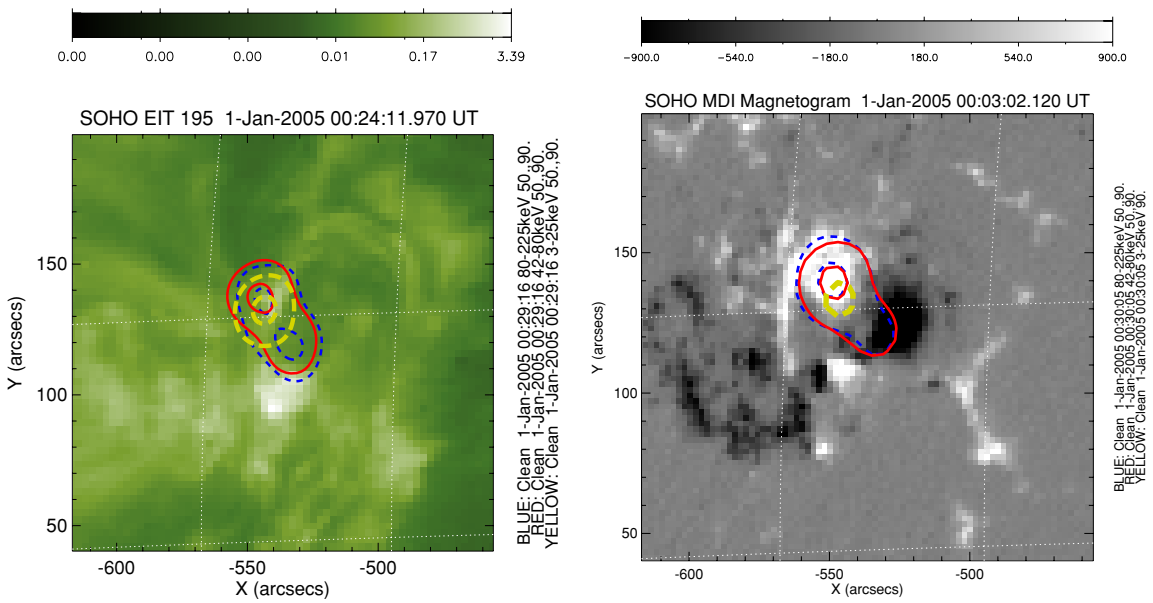

Figure 2. EIT 195 Å image (left panel) and longitudinal magnetic field observed by MDI (right panel) before the QPP in the 2005 January 1 flare. Superimposed are the contour levels at 50% and 90% of the maximum value of RHESSI images (reconstructed from collimators 4F–7F) (a) between 00:29:16 and 00:29:20 UT and (b) between 00:30:05 and 00:30:09 UT. Three energy ranges are shown: 3–25 keV in (yellow) thick long-dashed lines, 42–80 keV in (red) thin solid lines, and 80–225 keV in (blue) thin dashed lines.

(A color version of this figure is available in the online journal.)

or 40 points (NoRH), (2) applying an ideal filter with the passband of 0.01–0.1 Hz, or (3) applying a Gaussian filter with the half-width of 0.015–0.04 Hz. Periodograms of the light curves detrended by those techniques all have a well-pronounced spectral peak in the vicinity of 0.0245 Hz, i.e., a period of 41 s, in agreement with the visual inspection of the original light curves. The width of the spectral peak is about 3×10^{-3} Hz. A similar periodicity is detected in the autocorrelation curves for those observational channels.

The periodicity is not so pronounced in the 0.75–2 MeV SONG light curve, perhaps because of some instrumental problems. The periodicity is not seen in the RHESSI channels above 300 keV, where the count rates are insufficient in this event to allow the detection of modulations of depth over 25% out of the noise.

3.2. Cross-correlation Analysis

Figure 3 demonstrates the comparison of the microwave, hard X-ray, and gamma-ray time series. The time series are first detrended by subtracting the signals smoothed by 30 s (microwave) or about 32 s (hard X-ray and gamma-ray), and then smoothed by 12 s (microwave) or about 8 s (hard X-ray and gamma-ray). The time series are also normalized to their maxima. All three time series contain well-pronounced oscillations which are in phase with each other in the interval 00:28:20–00:30:50 UT (1,700 to 1,850 s), when the hard X-ray emission is strongest (see Figure 1). The cross-correlation coefficients for the microwave and hard X-ray, the microwave and gamma-ray curves and the hard X-ray and gamma-ray curves are 0.85, 0.72, and 0.78, respectively. In all three cases, the highest value of correlation is achieved for zero time lag, demonstrating very high correlation of the signals in all observational bands.

All three cross-correlation curves versus time lag show very clear harmonic oscillations with a period of about 40 s, in agreement with the above findings. The time mismatch of the three curves is within ±5 s and is not systematic. Thus, hard

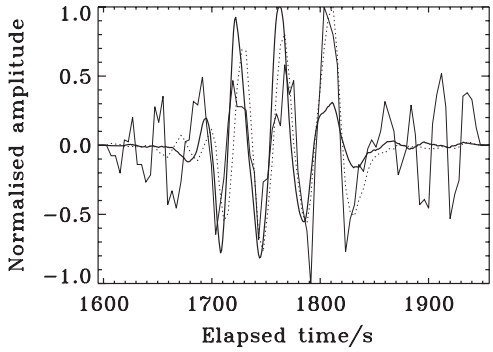

Figure 3. Detrended and smoothed microwave, hard X-ray, and gamma-ray time series of the analyzed flare, normalized to their maxima in the plotted interval (time is measured from 00:00 UT), for NoRH 34 GHz (thin solid), SONG 2–6 MeV (thick solid), and 80–225 keV (thick dashed).

X-ray and gamma-ray emissions are in phase in the interval from 1700 to 1850 s. In the whole time interval from 00:26:40 to 00:32:30 UT (1600–1950 s), the correlation coefficients are 0.85, 0.65, and 0.68, respectively.

The highest amplitude of gamma-ray QPP, as well as microwave and hard X-ray QPP, occurs when the total emission is highest (cf. Figures 1–3). The shorter period (about 25 s) pulsations seen in the 2–6 MeV channel before and after the main phase of the flare should be disregarded, as they are seen neither in other channels of SONG, nor with RHESSI or NoRH, and do not last longer than three periods. Moreover, the inspection of the original light curve in this channel (Figure 1(c)) does not show any oscillations above the noise level in the interval from 1600 s to 1660 s.

3.3. Spatial Structure of the Oscillations

Figure 4 shows snapshots, synthesized with RHESSI data, of the spatial structure of hard X-ray (42–80 keV) and low energy gamma-ray (80–225 keV) sources during the local extrema of the emission. The emission in both bands comes mainly

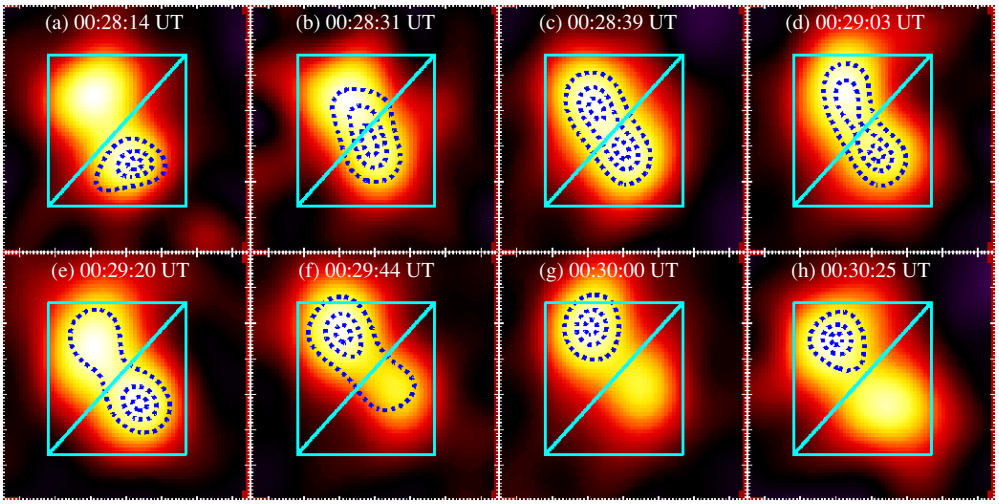

Figure 4. RHESSI images representative of the local extrema in the analyzed QPP shown in the 42–80 keV energy range with contour levels of 80–225 keV images in (blue) dashed lines (70%, 90%, and 98% of the maximum value). The images are reconstructed from collimators 4F-7F at the start time indicated in each image and for the shortest duration possible of about 4 s. The field of view for each image is centered on heliocentric coordinates $X = 530 \pm 35$ and $Y = 135 \pm 35$ arcsec. The triangular boxes overlaid separating the two footpoint sources indicate the areas over which the flux is averaged to produce the time series shown in Figure 5.

(A color version of this figure is available in the online journal.)

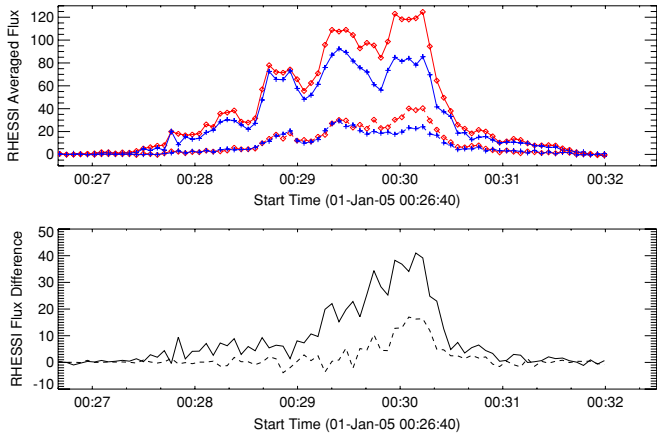

Figure 5. Sequence of QPP in separate sources in the time interval 00:26:40–00:32:30 UT, obtained from RHESSI images (reconstructed from collimators 4F-8F, see Figure 4) at energies of 42–80 keV (solid lines) and 80–225 keV (dashed lines). Upper panel: averaged flux for the upper and lower source, shown with diamonds (in red) and crosses (in blue), respectively. Bottom panel: flux difference between the upper and the lower source. The flux unit is in photons $\mathrm{cm}^{-2}\ \mathrm{s}^{-1}$.

(A color version of this figure is available in the online journal.)

from two spatially separated sources (or footpoints). The flux asymmetry in the strength of the sources evolves in time.

To investigate the evolution of the emission coming from the upper and lower sources, we divide the emitting region into two triangular areas with one common side situated along the neutral line. Figure 5 shows the time evolution of the averaged fluxes of hard X-rays (42–80 keV) and low energy gamma rays (80–225 keV) for each source. In both bands, QPP coming from both sources are almost in phase. The difference in flux between the sources grows in time with the development of the flare. The relative behavior of the gamma-ray sources is different: the averaged fluxes of the sources remain almost equal during all pulsations except one at 00:30:10 UT, when the upper source dominates.

The time evolution of the differences between the hard X-ray QPP in the upper and bottom sources is a gradually growing curve resembling the average light curve of the flare. In the developed phase of the flare, from 00:29:15 UT to 00:30:15 UT, the source difference flux oscillates with a period of about 13 s. The oscillations last for five cycles. Unfortunately, the oscillations are resolved very poorly, with only 3 or 4 points per period. However, as the oscillations are clearly seen in the signal, they can be considered as significant. The bottom panel shows that variations of the hard X-ray and gamma-ray footpoint emission differences are not necessarily in phase.

4. DISCUSSION AND CONCLUSIONS

The multi-wavelength multi-instrumental analysis of QPPs in a single loop solar flare on 2005 January 1 reveals the following:

1. QPPs with a period of about 40 s (the frequency of 0.025 ± 0.003 Hz), lasting for at least five cycles, observed in the microwave (17 GHz and 34 GHz) and hard X-ray (up to 100 keV) emission are also present in the gamma-ray emission at energies up to several MeV. In all observational channels, the QPPs have high modulation depth of about 20%–25%. The highest amplitude is reached when the total emission of the flare is highest.
2. Microwave and hard X-ray QPPs show a very high degree of correlation with each other, with the correlation coefficient higher than 80%, and zero time lag. Correlation of gamma-ray QPPs with microwave and hard X-ray QPPs is also high but not as strong (65%–70%). Thus, microwave, hard X-ray, and gamma-ray QPPs are found to be in phase.
3. Hard X-ray and low energy gamma-ray emissions come from two sources situated at the regions of opposite magnetic polarity. The location of sources remains approximately the same, and the hard X-ray and gamma-ray two-point sources evolve synchronously during all pulsations despite the spatial asymmetry. The flux difference between the hard X-ray sources grows in time, while the gamma-ray flux sources are almost identical except for one pulsation.
4. The difference between the averaged hard X-ray fluxes and gamma-ray fluxes coming from the two sources oscillates with a period of about 13 s for five cycles in the highest emission stage of the flare. The variations are not necessarily in phase between hard X-ray and gamma-ray energies.

The microwave emission and the hard X-ray emission are produced by non-thermal electrons, while gamma-ray emission is usually associated with non-thermal ions. Indeed, the gamma-ray part of the spectrum of the analyzed flare contains nuclear emission lines, confirming that the flare does produce accelerated ions. The synchronous QPPs of microwave and gamma-ray emission, revealed by our study, suggest that the electron and ion acceleration processes are likely to occur almost synchronously.

The 40 s gamma-ray QPPs are observed with SONG, but are not observed in similar gamma-ray channels of RHESSI, questioning their origin. However, the synchronous presence of the QPPs in microwaves and in the hard X-rays observed by both SONG and RHESSI proves that the gamma-ray QPPs are of solar origin and are indeed associated with the flare. Thus we attribute the lack of QPPs, detected with SONG, in the gamma-ray channels of RHESSI to their lower sensitivity.

The 40 s periodicity can be caused by several mechanisms. For example, the global sausage (fast magnetoacoustic) mode can create periodic precipitation of non-thermal electrons and ions by variation of the magnetic mirror ratio in the flaring loop (Zaitsev & Stepanov 1982). The large observed period suggests that the mode should be in the vicinity of the cut-off on the dispersion plot (Nakariakov et al. 2003; Pascoe et al. 2007). Hence, the period of the mode is determined by the ratio $2L/C_{\rm Ae}$ of the double the length of the loop, L, to the Alfvén speed, $C_{\rm Ae}$, outside the loop. For the observed distance between the footpoints, 21 Mm, $L \approx 33$ Mm. Hence, the observed periodicity requires $C_{\rm Ae}$ to be about 1600 km s^{-1}. This value is rather low, compared to previous estimates ranging from 3000 to 5000 km s^{-1} (e.g., Nakariakov et al. 2003; Melnikov et al. 2005; Inglis et al. 2008).

The 13 s oscillations of the difference between the hard X-ray fluxes coming from the two sources can be interpreted as the second harmonic of the sausage mode, excited by the energy release. The second sausage harmonic changes the magnetic field strength in the loop legs periodically and in anti-phase with each other. This leads to the periodic precipitation of non-thermal electrons at either footpoint. In this case, taking the wavelength to be equal to the loop length, we obtain an external Alfvén speed of about 2500 km s^{-1}. This value is significantly different from the estimation obtained for the global mode. The phase speeds of the global and second harmonics can be quite different because of dispersion. The phase speed of the sausage mode decreases with the increase in the mode number, which is in contradiction with the above interpretations. Thus, the 40 s and 13 s oscillations cannot be spatial harmonics of the same mode. Moreover, the phase variations between hard X-ray and gamma-ray for the two oscillations are different, pointing to a separate mechanism.

In fact, the phase speed of 1600 km s^{-1} required for the 40 s periodicity is close to the typical phase speeds of kink modes in coronal loops. We conclude that the considered QPPs are likely to be caused by magnetic reconnection and accompanying particle acceleration, periodically triggered by a global kink oscillation (Foullon et al. 2005; Nakariakov et al. 2006). The QPP can also be caused by self-induced regimes of repetitive magnetic reconnection (see Nakariakov & Melnikov 2009, for a review), but the lack of quantitative theory of these phenomena does not allow us to exclude or prove this possibility. The 13 s periodicity is likely to be the second harmonic of the sausage mode excited by the flare.

The quasi-periodic pulsation of gamma-ray emission in solar flares, found in this study, has interesting implications for the study of flaring energy releases and particle acceleration in them. A special interest is connected with the possible geoeffectiveness of such flares, which deserves a systematic study.

REFERENCES

Asai, A., Shimojo, M., Isobe, H., Morimoto, T., Yokoyama, T., Shibasaki, K., & Nakajima, H. 2001, ApJ, 562, L103
Aschwanden, M. J. 1987, Sol. Phys., 111, 113
Aschwanden, M. J. 2002, Space Sci. Rev., 101, 1
Chupp, E. L. 1983, Sol. Phys., 86, 383
Dauphin, C., Vilmer, N., Lüthi, T., Trottet, G., Krucker, S., & Magun, A. 2005, Adv. Space Res., 35, 1805
Delaboudinière, J.-P., et al. 1995, Sol. Phys., 162, 291
Foullon, C., Verwichte, E., Nakariakov, V. M., & Fletcher, L. 2005, A&A, 440, L59
Grechnev, V. V., White, S. M., & Kundu, M. R. 2003, ApJ, 588, 1163
Grigis, P. C., & Benz, A. O. 2004, A&A, 426, 1093
Inglis, A. R., & Nakariakov, V. M. 2009, A&A, 493, 259
Inglis, A. R., Nakariakov, V. M., & Melnikov, V. F. 2008, A&A, 487, 1147
Jin, M., & Ding, M. D. 2007, A&A, 471, 705
Kliem, B., Karlický, M., & Benz, A. O. 2000, A&A, 360, 715
Lin, R. P., et al. 2002, Sol. Phys., 210, 3
Melnikov, V. F., & Magun, A. 1998, Sol. Phys., 178, 153
Melnikov, V. F., Reznikova, V. E., Shibasaki, K., & Nakariakov, V. M. 2005, A&A, 439, 727
Murray, M. J., van Driel-Gesztelyi, L., & Baker, D. 2009, A&A, 494, 329
Myagkova, I. N., Kuznetsov, S. N., Kurt, V. G., Yuskov, B. Y., Galkin, V. I., Muravieva, E. A., & Kudela, K. 2007, Adv. Space Res., 40, 1929
Myagkova, I. N., Kuznetsov, S. N., Muravieva, E. A., & Starostin, L. I. 2007, in Modern Solar Facilities-Advanced Solar Science, ed. F. Kneer, K. G. Puschmann, & A. D. Wittmann (Göttingen: Univ. Göttingen), 281
Nakajima, H., et al. 1994, Proc. IEEE., 82, 705
Nakariakov, V. M. 2007, Adv. Space Res., 39, 1804
Nakariakov, V. M., Foullon, C., Verwichte, E., & Young, N. P. 2006, A&A, 452, 343
Nakariakov, V. M., & Melnikov, V. F. 2009, Space Sci. Rev., 55
Nakariakov, V. M., Melnikov, V. F., & Reznikova, V. E. 2003, A&A, 412, L7
Ofman, L., & Sui, L. 2006, ApJ, 644, L149
Parkhomov, V. A., Moldavanov, A. V., & Tsegmed, B. 2006, J. Atmos. Sol.-Terr. Phys., 68, 1370
Pascoe, D. J., Nakariakov, V. M., & Arber, T. D. 2007, A&A, 461, 1149
Scherrer, P. H., et al. 1995, Sol. Phys., 162, 129
Zaitsev, V. V., & Stepanov, A. V. 1982, Sov. Astron. Lett., 8, 132